

Stability and melting behavior of boron phosphide under high pressure

Wenjia Liang(梁文嘉), Xiaojun Xiang(向晓君), Qian Li(李倩), Hao Liang(梁浩), and Fang Peng(彭放)

Citation: Chin. Phys. B, 2024, 33 (**4**): 046201. DOI: 10.1088/1674-1056/ad23d4
Journal homepage: http://cpb.iphy.ac.cn; http://iopscience.iop.org/cpb

What follows is a list of articles you may be interested in

Chair-like N_6^{6-} in AlN_3 with high-energy density

Shi-Tai Guo(郭世泰), Zhen-Zhen Xu(徐真真), Yan-Lei Geng(耿延雷), Qi Rui(芮琦), Dian-Chen Du(杜殿臣), Jian-Fu Li(李建福), and Xiao-Li Wang(王晓丽)

Chin. Phys. B, 2023, 32 (**12**): 126202. DOI: 10.1088/1674-1056/acfd1a

High-pressure study of topological semimetals XCd_2Sb_2 (X = Eu and Yb)

Chuchu Zhu(朱楚楚), Hao Su(苏豪), Erjian Cheng(程二建), Lin Guo(郭琳), Binglin Pan(泮炳霖), Yeyu Huang(黄烨煜), Jiamin Ni(倪佳敏), Yanfeng Guo(郭艳峰), Xiaofan Yang(杨小帆), and Shiyan Li(李世燕)

Chin. Phys. B, 2022, 31 (**7**): 076201. DOI: 10.1088/1674-1056/ac7212

Reaction mechanism of metal and pyrite under high-pressure and high-temperature conditions and improvement of the properties

Yao Wang(王遥), Dan Xu(徐丹), Shan Gao(高姗), Qi Chen(陈启), Dayi Zhou(周大义), Xin Fan(范鑫), Xin-Jian Li(李欣健), Lijie Chang(常立杰),Yuewen Zhang(张跃文), Hongan Ma(马红安), and Xiao-Peng Jia(贾晓鹏)

Chin. Phys. B, 2022, 31 (**6**): 066206. DOI: 10.1088/1674-1056/ac4a72

Theoretical study of novel B-C-O compoundswith non-diamond isoelectronic

Chao Liu(刘超) and Pan Ying(应盼)

Chin. Phys. B, 2022, 31 (**2**): 026201. DOI: 10.1088/1674-1056/ac0cd2

Insights into the physical properties and anisotropic nature of ErPdBi with an appearance of low minimum thermal conductivity

S K Mitro, R Majumder, K M Hossain, Md Zahid Hasan, Md Emran Hossain, and M A Hadi

Chin. Phys. B, 2021, 30 (**1**): 016203. DOI: 10.1088/1674-1056/abaf9d

---

Stability and melting behavior of boron phosphide under high pressure

Wenjia Liang(梁文嘉)[1], Xiaojun Xiang(向晓君)[1], Qian Li(李倩)[1], Hao Liang(梁浩)[2,3,‡], and Fang Peng(彭放)[1,†]

[1] *Institute of Atomic and Molecular Physics, Sichuan University, Chengdu* 610065, *China*
[2] *School of Mathematics and Physics, Southwest University of Science and Technology, Mianyang* 621900, *China*
[3] *Center for High Pressure Science and Technology Advanced Research (HPSTAR), Shanghai* 201203, *China*

(Received 16 October 2023; revised manuscript received 11 January 2024; accepted manuscript online 30 January 2024)

Boron phosphide (BP) has gained significant research attention due to its unique photoelectric and mechanical properties. In this work, we investigated the stability of BP under high pressure using x-ray diffraction and scanning electron microscope. The phase diagram of BP was explored in both B-rich and P-rich environments, revealing crucial insight into its behavior at 5.0 GPa. Additionally, we measured the melting curve of BP from 8.0 GPa to 15.0 GPa. Our findings indicate that the stability of BP under high pressure is improved within B-rich and P-rich environments. Furthermore, we report a remarkable observation of melting curve frustration at 10.0 GPa. This study will enhance our understanding of stability of BP under high pressure, shedding light on its potential application in semiconductor, thermal, and light-transmitting devices.

Keywords: boron phosphide, stability, melting curve, high pressure

PACS: 62.50.–p, 64.70.dj, 81.10.–h, 74.62.Bf **DOI:** 10.1088/1674-1056/ad23d4

1. Introduction

Boron phosphide (BP) is renowned for its zinc-blende crystal structure and an array of remarkable electrical, thermal, and mechanical properties. It has received a great deal of attention of researchers and garnered significant efforts due to its exceptional attributes.[1–4] BP emerges as a semiconductor material possessing a wealth of advantageous characteristics. With a moderate band gap of 2.01 eV, it stands as an appealing candidate for neutron detection applications and can be doped to manifest n- or p-type conductivity with resistivity spanning from 10^{-2} Ω·cm to 10^{2} Ω·cm.[5–8] Furthermore, BP exhibits high transmittance in the infrared spectrum, rendering it a valuable material for optical coatings.[7–9] Notably, it emerges as a potential electrode material for water splitting applications,[8–10] showcasing its multifaceted utility. The versatility of material extends to its thermal properties, where it shines as an exceptionally efficient thermal conductor. With an extraordinarily high thermal conductivity ranging from 460 W/m·K to 540 W/m·K, BP has gained attention for its application in thermal properties.[11–13] Its thermal stabilities, impressive at 1130 °C, position it favorably in high-temperature environments.[14–16] Additionally, BP boasts impressive mechanical strength, boasting a Vicker's hardness of 30 GPa and an elastic modulus of 362 GPa, highlighting its robustness and durability.[17] The physical attributes and practical applications of BP will spur substantial experimental and theoretical investigations.

As a versatile structural material with practical applications, it becomes imperative to conduct a comprehensive exploration about the stability of BP across diverse environmental conditions. Various synthesis techniques, including chemical vapor deposition (CVD) and melt growth methods, have been employed to synthesize BP.[14–16,18,19] Nevertheless, the stability of BP is always lacking in extensive research concerning under high pressure. Despite its reputation as a highly stable substance, BP gradual decomposes into boron subphosphide ($B_{12}P_2$) only at temperatures above 1130 °C. BP remains remarkable stability beyond 2.0 GPa and 1200 °C.[2,20,21] There have been *ab initio* calculations that disclosed three distinct phases of BP: $F\bar{4}3m$, $C2/m$, and $P42/mmm$. Among them, the $F\bar{4}3m$ phase remains stable up to 113 GPa.[22] Furthermore, investigations of Kulnitskiy *et al.* have uncovered a rhombohedral structure in BP using high-resolution transmission electron microscopy.[23] In addition, Solozhenko and Mukhanov[20] have determined the melting temperature of BP to exceed 2400 °C at 2.6 GPa, displaying a negative slope melting curve of -60 ± 7 °C/GPa. Undoubtedly, comprehending stabilities of BP are essential for its widespread practicality. Regrettably, the behavior of BP's stability under high pressure has garnered insufficient attention.

In this study, we conducted high-pressure and high-temperature (HPHT) experiments using the DS6×14 MN and DS6×8 MN cubic press. Our investigations found two critical aspects: Firstly, we performed a comprehensive analysis of BP's behavior within B-rich and P-rich environments at

†Corresponding author. E-mail: pengfang@scu.edu.cn
‡Corresponding author. E-mail: lh910518@126.con

© 2024 Chinese Physical Society and IOP Publishing Ltd

5.0 GPa. Secondly, we scrutinized the melting behavior of BP at HPHT. In the first aspect, we constructed a phase diagram for BP at 5.0 GPa, uncovering an insight: the stability of BP under high pressure will be improved within B-rich and P-rich environment. In the second aspect, we systematically summarized the melting curve of BP under pressure. Our findings unveiled that BP exhibits a strong stability until it melts under HPHT. Remarkably, we found a melting curve frustration emerged at 10.0 GPa. The determination of phase composition and transitions was accomplished through x-ray diffraction (XRD). Meanwhile, the refinement of crystal structures was executed using the Rietveld method, facilitated by the GSAS program analysis.[24,25] Scanning electron microscopy (SEM) images were used to provide the microstructure, particle size, and compositional uniformity of recovered samples.

2. Experiment method

2.1. Specimen preparation

The raw materials of boron (B) and phosphorus (P) with a purity 99% were commercially purchased from Alfa Asear Co., Inc. The raw materials of BP were prepared according to Ref. [6]. The XRD patterns and SEM images of raw powders are shown in Fig. S1 in the supporting information. The precursors were mixed with BP and either P or B, with the molar ratios of B/P elements from 1:2 to 12:1.

2.2. Synthesis experiments and BP stability experiments

The synthesis experiments were conducted using a DS6×14 MN cubic press (5.0 GPa).[26,27] An A-type assembly equipped with a pyrophyllite cube was used. The pressure and temperature of the assembly were calibrated prior to the experiment. Particularly, the pressure was calibrated by the phase transition pressures of Bi, Tl and Ba. The temperature at 5.0 GPa was calibrated by $Pt_{97}Rh_3$–$Pt_{70}Rh_{30}$ thermocouple (30–1800 °C) and $W_{97}Re_3$–$W_{75}Re_{25}$ thermocouple (800–2200 °C). The precursors were held for 30 min at the desired pressure and temperature. Detailed information can be found in Refs. [28–35].

The experiments on BP stability from 8.0 GPa to 15.0 GPa were carried out using DS6×8MN cubic press. A 14–8 assembly was utilized, which had WC anvils featuring an 8 mm truncation edge length and a MgO octahedron possessing an edge length of 14 mm. The pressure and temperature of the assembly were calibrated prior to the experiment. Specifically, the pressure was calibrated by the phase transition pressures of Bi, ZnTe, and ZnS at room temperature. The temperature for each pressure (8.0 GPa, 10.0 GPa, 12.0 GPa, and 15.0 GPa) was calibrated by $W_{97}Re_3$–$W_{75}Re_{25}$ thermocouple. Detailed information was described in Refs. [30,36–39].

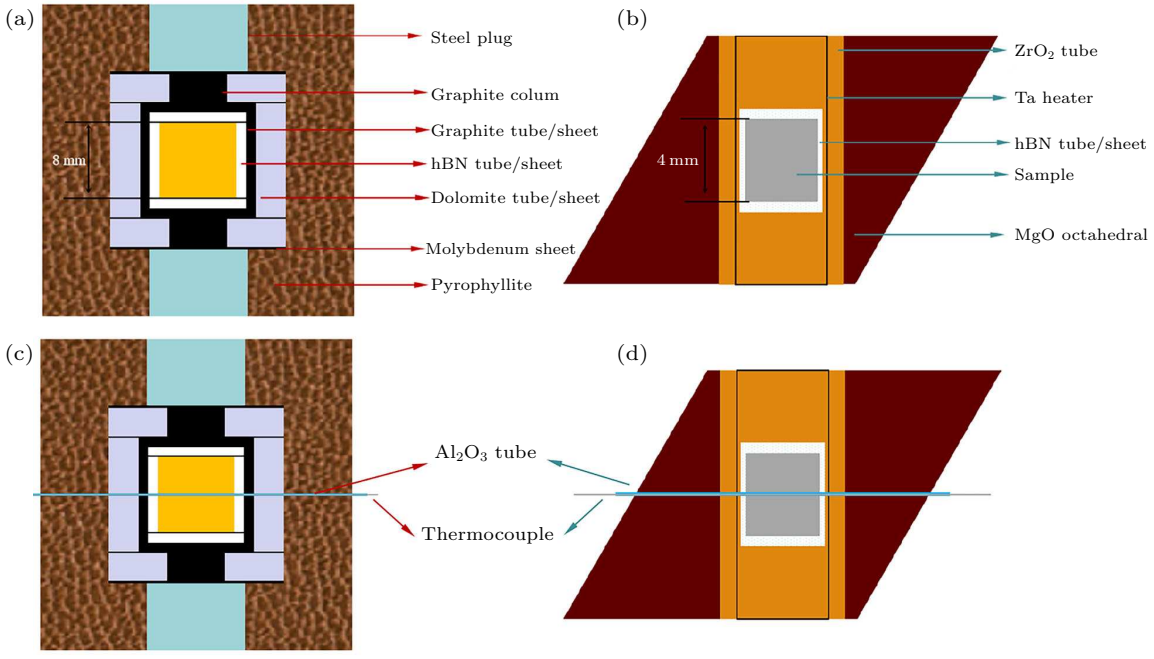


Fig. 1. (a) Sectioned view of the A-type assembly. (b) Sectioned view of the 14–8 assembly. (c) Thermocouple insertion position in the A-type assembly. (d) Thermocouple insertion position in the 14–8 assembly.

2.3. *In situ* high pressure temperature measurement method

The *in situ* high pressure temperature measurement method[30,40] was used for measuring melting temperature. The thermocouple penetrated the furnace and pressure medium (pyrophyllite cube or MgO octahedral) with their junctions inside the furnace and was protected by an alumina tubing (Al_2O_3). The thermocouple was in direct contact with water-cooling WC faces via soft copper end plugs without cold-junction compensation. The heating power was linearly

increased as a function of the time via a multi-channel data recorder designed to continuously monitor and record the temperature signals. The temperature error was approximately ±2°. The A-type and 14–8 assembly with their thermocouple insertion diagrams are shown in Fig. 1.

2.4. Sample characterization

The phase composition of the recovered samples was characterized by x-ray diffraction (XRD; DX-2700, Dandong) using Cu K_α-I radiation. The crystal structure and other refined parameters, including phase compositions, lattice parameters, grain sizes and deviatoric strain, were derived using the GSAS program within the EXPGUI software package.[25,41] The surface image of the recovered samples was observed by a scanning electron microscope (SEM; JSM-IT500, JEOL).

3. Results and discussion

3.1. Stability in B-rich and P-rich environments

The high-pressure synthesis experiments were conducted at 5.0 GPa and 800–2200 °C. The evolution and formation of precursors are illustrated in Fig. 2(a), unveiling two distinct phenomena. For B_{mol}: $P_{mol} < 0.5$, only BP with P is observed, devoid of any new compounds. In contrast, recovered samples with B_{mol}: $P_{mol} > 0.5$ at 1600 °C display a new phase $B_{12}P_2$, whose decomposition temperature at ambient pressure is 1130 °C. Interestingly, the old phase BP hardly disappears in B-rich environments even at temperature up to 2300 °C in Fig. S3. Notably, excessive B can weaken the content of BP according to the diffraction peaks and the same phenomenon occurs in WB_4.[29] In previous experiments,[6] the synthesis temperature is at 800 °C. Therefore, the phase diagram of BP is depicted in Fig. 2(d). The phase diagram illustrates two reaction lines for BP: the BP reaction line, starting at 800 °C and covering the entire phase range, and the $B_{12}P_2$ reaction line, initiating at 1600 °C, but only manifesting in B-rich environments.

The melting temperature measurement experiments of P are illustrated in Fig. 2(c). Initially, the temperature values increase with the heating rate of 10 W/min. based on the heat absorption of the melting process, there will be a temperature plateau. We measured the temperature of these three samples: $B_{mol} : P_{mol} = 1 : 4$, $B_{mol} : P_{mol} = 1 : 2$, and black P. All plateaus of the three temperature curves are at 1083.3 ± 1.8° (1083 °C, 1086 °C, and 1081 °C, respectively). Based on some reports of eutectic reaction,[42,43] the plateaus are the melting temperature of P, and BP does not affect the melt of P. BP + P transforms into BP + liquid phosphorus (BP + L) when crossing this plateau. The phase diagram is only plotted up to 2100 °C.

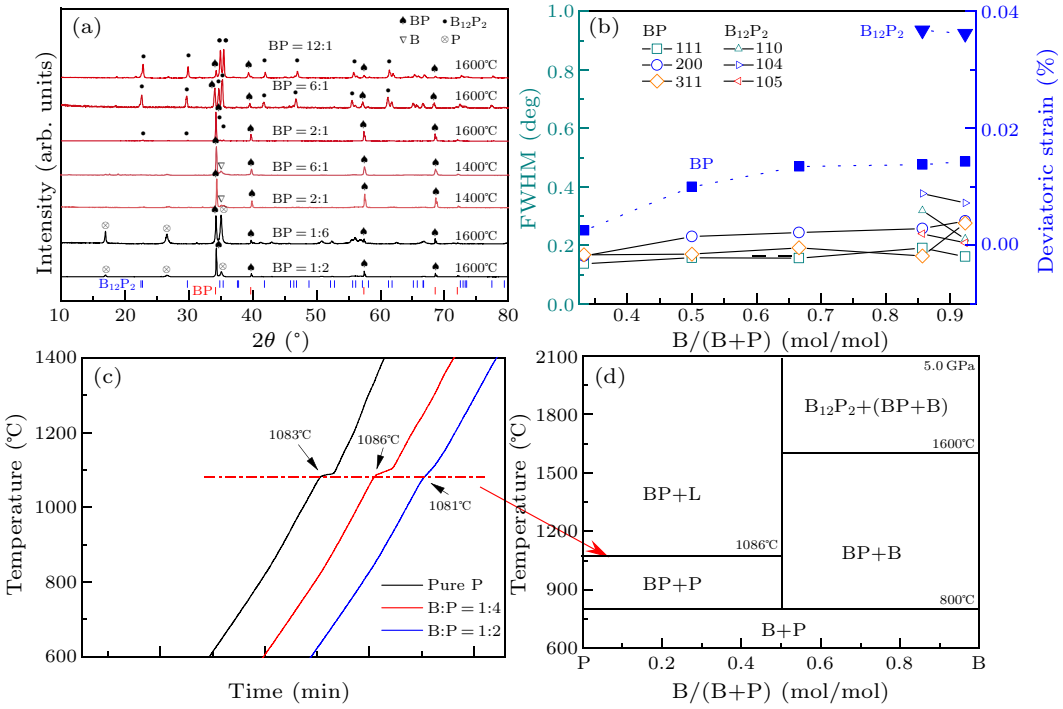


Fig. 2. (a) XRD patterns of recovered samples with different B/P atomic ratios and temperatures at 5.0 GPa. (b) Relationship between deviatoric strain and the corresponding FWHM of typical planes and B/P molar ratio at 5.0 GPa and 1600 °C. (c) The thermal property measurements conducted with a heating rate of 0.01 kW/min at 5.0 GPa. All plateaus, pure P, B : P = 1 : 4, and B : P = 1 : 2, occur at 1083.3 ± 1.6°. (d) The phase diagram of BP at 5.0 GPa.

Figure 3(a) shows that the BP grain size remains constant at 30–50 μm in a P-rich environment, similar to the initial BP powder. P surrounds BP grains in a molten state, with a distinct boundary. In Fig. 3(b), we observed an abundance of small grains alongside a smaller number of large grains. The large grains, with a size of 10 μm, are BP crystals, while

smaller ones about 1 μm correspond to $B_{12}P_2$. Intriguingly, the grain boundaries of BP and $B_{12}P_2$ partially adhere to each other. Figure 2(b) illustrates the full width at half maximum (FWHM) and deviatoric strain of recovered sample at different molar ratios. The deviatoric strain of BP is rapidly elevated with the increase of B and then stabilizes at a 0.7 molar ratio, meanwhile the deviatoric strain of $B_{12}P_2$ is quite higher from the outset of its appearance. With the production of $B_{12}P_2$, the deviatoric strain of BP will increase due to the high hardness materials of $B_{12}P_2$. Figures 3(c) and 3(d) present the Rietveld-refined XRD patterns for the BP samples and the recovered samples with $B_{mol} : P_{mol} = 12 : 1$ at 5.0 GPa and 1600 °C. The unit cell parameters of BP and $B_{12}P_2$ are summarized in Table S1. Within a B-rich environment, the lattice of BP is in compression.

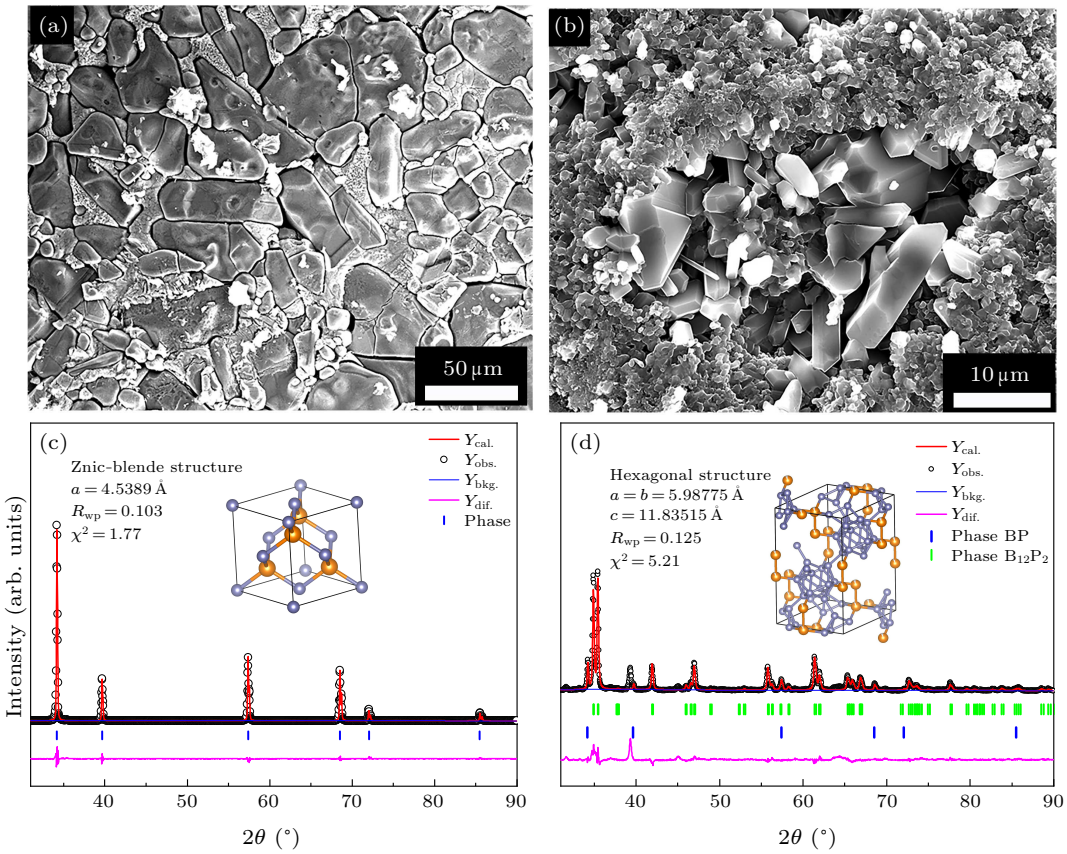


Fig. 3. (a) Recovered sample with $B_{mol} : P_{mol} = 1 : 2$ at 5.0 GPa and 1600 °C. (b) Recovered sample with $B_{mol} : P_{mol} = 12 : 1$ at 5.0 GPa and 1600 °C, $B_{12}P_2$ is fine grains and BP is large grains. Rietveld-refined XRD pattern ($\lambda = 0.154059$ Å) of BP: (c) initial powder: $a = 4.5389$ Å, $R_{wp} = 0.103$, $\chi^2 = 1.77$; (d) recovered sample with $B_{mol} : P_{mol} = 12 : 1$ at 5.0 GPa and 1600 °C: $B_{12}P_2$, $a = b = 5.987$ Å, $c = 11.835$ Å and BP, $a = b = c = 4.5342$ Å, $R_{wp} = 0.125$, $\chi^2 = 5.21$.

3.2. Melting behavior of pure-phase BP

Stability measurements on BP with a grain size of 30–50 μm were undertaken under HPHT, with the pressure ranging from 8.0 GPa to 15.0 GPa. The investigations revealed a high stability of BP, with the structure exhibiting not changing up to its melting temperature. The XRD patterns of BP under HPHT are presented in Fig. S4. No distinctive phase transitions were observed under HPHT.

Although no distinct phase transitions were observed under HPHT conditions, our examination of BP melting behavior unveiled a significant transition. The temperatures were measured by $W_{97}Re_3$–$W_{75}Re_{25}$ thermocouple with heating rate of 75 W/min. As the BP melted, the temperature quickly levelled off in Fig. 4(c). After the emergence of the melting plateau at 1968 °C, we stopped the heating process. By the way, BP at 10.0 GPa and 1800 °C is not melted with crystal sizes of 30–50 μm in Fig. S5(a). Therefore, the melting plateaus are seen as the melting temperature of BP, with the temperature plateau held constant for three repetitions at each pressure. The melting temperatures of BP at 10.0 GPa, 12.0 GPa, and 15.0 GPa are 1968 °C, 1950 °C, and 1940 °C, respectively. In Fig. 4(a), XRD analysis of recovered samples revealed marked difference in the diffraction peak intensity between the melted samples and the sintered body. The strongest peaks at 10.0 GPa, 12.0 GPa, and 15.0 GPa correspond to the (111), (111), and (311) planes, respectively. Figure 4(b) presents the SEM images capturing BP's melting at 12.0 GPa, revealing the melting texture clearly. The fastest cooling rate at the very surface of the BP, which results in the formation of nanocrystalline regions during solidification in Fig. 4(d).[44,45] As the

solidification progresses towards the interior, the cooling rate decreases, making BP transform from nanocrystalline solidification to dendritic solidification. The demarcation line between nanocrystalline and dendrite solidification is visible in Fig. 4(e). By the way, these dendritic grains exhibit selective orientations, which are mainly responsible for the asymmetry of the XRD patterns in Fig. 4(a). As the cooling rate drops further in inside, the BP solidifies as coarse equiaxed grains. Figure 4(f) shows a more noticeable dendritic morphology, as well as a few equiaxed grains on the right side.

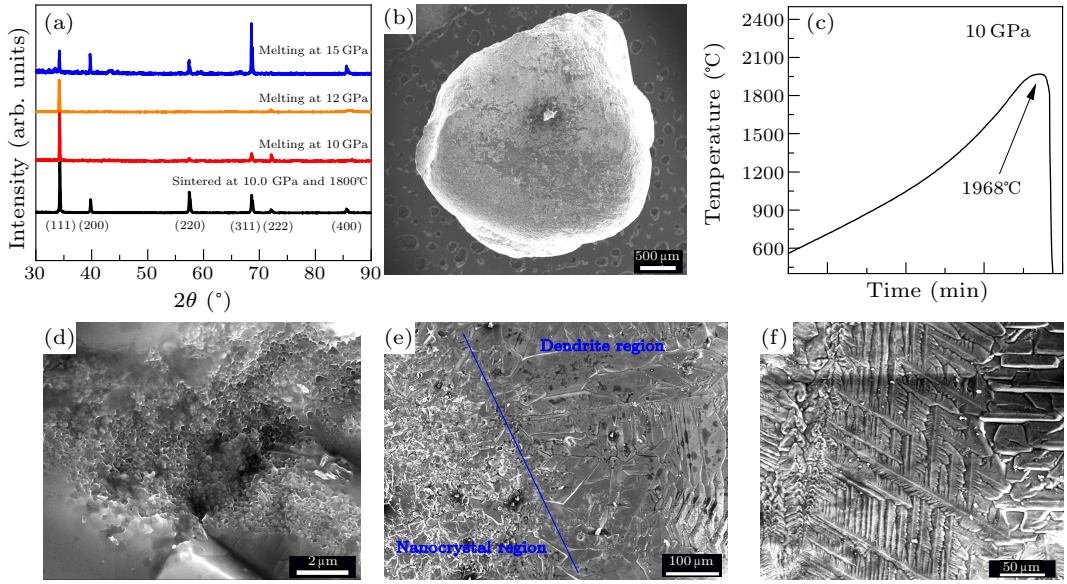


Fig. 4. (a) XRD patterns of melt samples and sintered body. (b) The SEM image of recovered sample at 12.0 GPa. (c) The thermal property measurements conducted with a heating rate of 75 W/min at 10.0 GPa. (d) The fine crystal region. (e) The junction of dendrite region and nanocrystal region. (f) The dendrite region.

We also conducted sintering experiments of BP at 5.0 GPa to verify the melting temperature in the report of Solozhenko and Mukhanov[20]. Because the $W_{97}Re_3$–$W_{75}Re_{25}$ thermocouple fails in this temperature range, the melting behavior of BP was observed by SEM in Fig. S5. The surface morphology of the recovered sample was observed by holding at 2300 °C for 1 min and then quenching to room temperature, where signs of melting were clearly visible. The melting temperature in the report of Solozhenko and Mukhanov[20] is 2269 °C and our results are in agreement with his work.

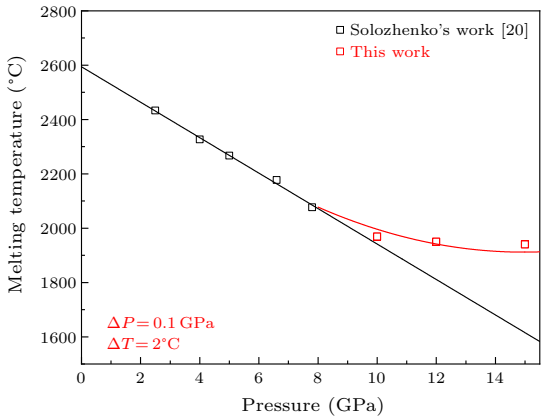


Fig. 5. The melting curve of BP at high pressure.

Figure 5 demonstrates that the melting curve of BP cannot be fitted linearly after 10.0 GPa. Therefore, a quadratic fit combined with the data of Solozhenko and Mukhanov[20] was performed in this work. The BP melting curve can be fitted as follows:

$$T_{\mathrm{m}} = aP^2 + bP + c, \tag{1}$$

where $a = 3.4 \pm 0.3$ °C/GPa^2, $b = -102.4 \pm 6.7$ °C/GPa, and $c = 2677.9 \pm 29.1$ °C/GPa. Ross *et al.*[46,47] found that the formation of localized bonds results in a reduction in the melting energy. In a parallel study, Gui *et al.*[14] revealed a gradual increase in covalent bonds within BP under high pressure and reaches a maximum at 10.0 GPa. Therefore, we postulated that the frustration of the melting temperature of BP at 10.0 GPa is closely related to a shift in the bond valence within BP.

4. Conclusions

In summary, we have successfully determined the phase diagram of BP. Our results indicate that the stability of BP under high pressure can be improved within B-rich and P-rich environments. The compressed state of BP under high pressure creates ideal conditions for impeding B entering into BP. The melting curve of BP exhibits a quadratic shape, with a frustration in the BP melting curve at 10.0 GPa, which may be related to a shift in the bond valence within BP. These results highlight the remarkable temperature stability and excellent chemical resistance of BP, making BP a promising material for industrial applications.

Acknowledgments

Project supported by the National Natural Science Foundation of China (Grant No. 12074273) and the Sichuan Science and Technology Program (Grant No. 2022NSFSC1810).

References

[1] Wettling W and Windscheif J 1984 *Solid State Commun.* **50** 33
[2] Ananthanarayanan K P, Mohanty C and Gielisse P J 1973 *J. Cryst. Growth* **20** 63
[3] Deb J and Sarkar U 2021 *Appl. Surf. Sci.* **541** 148657
[4] Munsif S, Khan S, Ali A, Gilani M A, Iqbal J, Ludwig R and Ayub K 2018 *J. Mol. Liq.* **271** 51
[5] Lund J C, Olschner F, Ahmed F and Shah K S 1989 *MRS Online Proc. Libr. OPL* **162** 601
[6] Liang W, Zhang L, Xiang X, Wang J, Zhang L, Wu B, Wang Y, Zeng Y, Guan S and Tang Q 2021 *Solid State Commun.* **327** 114206
[7] Varley J B, Miglio A, Ha V-A, van Setten M J, Rignanese G-M and Hautier G 2017 *Chem. Mater.* **29** 2568
[8] Shi L, Li P, Zhou W, Wang T, Chang K, Zhang H, Kako T, Liu G and Ye J 2016 *Nano Energy* **28** 158
[9] Gibson D R, Waddell E M, Wilson S A and Lewis K L 1994 *Opt. Eng.* **33** 957
[10] Mou S, Wu T, Xie J, Zhang Y, Ji L, Huang H, Wang T, Luo Y, Xiong X and Tang B 2019 *Adv. Mater.* **31** 1903499
[11] Zheng Q, Li S, Li C, Lv Y, Liu X, Huang P Y, Broido D A, Lv B and Cahill D G 2018 *Adv. Funct. Mater.* **28** 1805116
[12] Jiajun H, Kai W, Xinguang H, Ting Y and Hongyan X 2022 *J. Inorg. Mater.* **37** 933
[13] Kang J S, Wu H and Hu Y 2017 *Nano Lett.* **17** 7507
[14] Gui R, Xue Z, Zhou X, Gu C, Ren X, Cheng H, Ma D, Qin J, Liang Y and Yan X 2020 *Phys. Rev. B* **101** 035302
[15] Kumashiro Y, Yao T and Gonda S 1984 *J. Cryst. Growth* **70** 515
[16] Kumashiro Y 1990 *J. Mater. Res.* **5** 2933
[17] Solozhenko V L and Bushlya V 2019 *J. Superhard Mater.* **41** 84
[18] Popper P and Ingles T A 1957 *Nature* **179** 1075
[19] Perri J A, La Placa S and Post B 1958 *Acta Crystallogr.* **11** 310
[20] Solozhenko V L and Mukhanov V A 2015 *J. Superhard Mater.* **37** 438
[21] Peret J L 1964 *J. Am. Ceram. Soc.* **47** 44
[22] Zhang X, Qin J, Liu H, Zhang S, Ma M, Luo W, Liu R and Ahuja R 2015 *Sci. Rep.* **5** 8761
[23] Kulnitskiy B A, Blank V D, Gordeeva T A, Mukhanov V A and Solozhenko V L 2022 *Solid State Commun.* **354** 114886
[24] Tang Y, Zhang Q, Lou H, Tan L, Tian Y, Guan S, Wang W, Huang M, Zeng Q and He D 2021 *J. Alloys Compd.* **886** 161239
[25] Rodríguez-Carvajal J 1993 *Physica B* **192** 55
[26] Wang S, He D, Wang W and Lei L 2009 *High Press. Res.* **29** 806
[27] Wang Y, Tang Y, Kou Z and He D 2023 *Int. J. Refract. Met. Hard Mater.* **110** 106015
[28] Zhou X, Ma D, Wang L, Zhao Y and Wang S 2020 *Rev. Sci. Instrum.* **91** 015118
[29] Wang W, Peng F, Liang H, Guan S, Liang W, Zhang L, Huang M, Tang Y and He D 2022 *Int. J. Refract. Met. Hard Mater.* **102** 105701
[30] Wang J, He D, Li X, Zhang J, Li Q, Wang Z, Su Y, Tian Y, Yang J and Peng B 2020 *Solid State Commun.* **307** 113805
[31] Gunasekaran S and Anbalagan G 2007 *Bull. Mater. Sci.* **30** 339
[32] Engler P, Santana M W, Mittleman M L and Balazs D 1989 *Thermochim. Acta* **140** 67
[33] Liang A, Liu Y, Liang H, Liu F, Fan C, Zhang J, Wu J, Chen J and He D 2018 *High Press. Res.* **38** 458
[34] An P, He Z, Qin J, Li Z, Li Y, Kou Z and He D 2011 *J. Wuhan Univ. Technol. Mater. Sci. Ed.* **26** 914
[35] Qin J, He D, Lei L, An P, Fang L, Li Y, Wang F and Kou Z 2009 *J. Alloys Compd.* **476** L8
[36] Wang F L, He D W, Fang L M, Chen X F, Li Y J, Zhang W, Zhang J, Kou Z L and Peng F 2008 *Acta Phys. Sin.* **57** 5429 (in Chinese)
[37] Wang W D, He D W, Wang H K, Wang F L, Dong H N, Chen H H, Li Z Y, Zhang J, Wang S M, Kou Z L and Peng F 2010 *Acta Phys. Sin.* **59** 3107 (in Chinese)
[38] Wang W D, He D w, Tang M j, Li F j, Liu L and Bi Y 2012 *Diam. Relat. Mater.* **27** 49
[39] Wang J, Tian Y, Su Y, Xiang X, Zhou L, Huang M, Zhang L and He D 2023 *CrystEngComm* **25** 1884
[40] McDaniel M L, Babb Jr S E and Scott G J 1962 *J. Chem. Phys.* **37** 822
[41] Xiang X J, Song G Z, Zhou X F, Liang H, Xu Y, Qin S J, Wang J P, Hong F, Dai J H and Zhou B W 2020 *Chin. Phys. B* **29** 088202
[42] Li C, Li Q, Li Y, She X, Cao H, Zhang P, Wang L and Ding Y 2019 *Appl. Energy* **238** 1074
[43] Chipman J 1972 *Metall. Mater. Trans. B* **3** 55
[44] Liang A, Liu Y, Shi L, Lei L, Zhang F, Hu Q and He D 2019 *Phys. Rev. Res.* **1** 033090
[45] Hrubiak R, Meng Y and Shen G 2017 *Nat. Commun.* **8** 14562
[46] Ross M, Boehler R and Errandonea D 2007 *Phys. Rev. B* **76** 184117
[47] Ross M, Errandonea D and Boehler R 2007 *Phys. Rev. B* **76** 184118